

Successive Decode-and-Forward Relaying with Reconfigurable Intelligent Surfaces

Zaid Abdullah, Steven Kisseleff, Konstantinos Ntontin, Wallace Alves Martins, Symeon Chatzinotas, and Björn Ottersten

Interdisciplinary Centre for Security, Reliability and Trust (SnT), University of Luxembourg, Luxembourg.
E-mails: {zaid.abdullah, steven.kisseleff, kostantinos.ntontin, wallace.alvesmartins, symeon.chatzinotas, bjorn.ottersten}@uni.lu

Abstract—The key advantage of successive relaying (SR) networks is their ability to mimic the full-duplex (FD) operation with half-duplex (HD) relays. However, the main challenge that comes with such schemes is the associated inter-relay interference (IRI). In this work, we propose a reconfigurable intelligent surface (RIS)-enhanced SR network, where one RIS is deployed near each of the two relay nodes to provide spatial suppression of IRI, and to maximize the gain of desired signals. The resultant max-min optimization problem with joint phase-shift design for both RISs is first tackled via the semidefinite programming (SDP) approach. Then, a lower-complexity solution suitable for real-time implementation is proposed based on particle swarm optimization (PSO). Numerical results demonstrate that even relatively small RISs can provide significant gains in achievable rates of SR networks, and the proposed PSO scheme can achieve a near optimal performance.

Index Terms—Successive relaying, reconfigurable intelligent surface, decode-and-forward, particle swarm optimization, semidefinite programming.

I. INTRODUCTION

Successive relaying (SR) is a well known technique in wireless communication, where two half-duplex (HD) relays simultaneously assist the transmission between a source and destination nodes utilizing the full bandwidth, and thus imitating full-duplex (FD) operation [1]. The main idea is that at a given time-instant, the source transmits data to one relay, and simultaneously, the other relay forwards the data that it received from the source in the previous transmission time-instant to the destination. Hence, it becomes quite clear that a main challenge in realizing such a scheme is inter-relay interference (IRI). Thus far, authors have adopted different approaches to deal with IRI, such as channel ordering and rate adaptation [2], relay interference cancellation and precoding [3], or by neglecting IRI assuming fixed directional relays or large distance between active relays [4].

However, the recently proposed reconfigurable intelligent surfaces (RISs) can be a game changer for many wireless applications, including SR as we will demonstrate in this paper. Thanks to their ability in tweaking the wireless environment while maintaining low cost and power requirements, RISs have gained much attention as a strong candidate for future wireless networks [5]–[8]. In principle, RISs are similar to FD amplify-and-forward relaying, with the former providing passive beamforming without the need to include active power

amplifiers or radio-frequency chains, while the latter has the ability to provide active amplification at the cost of increased hardware complexity and power consumption.

Instead of dealing with conventional active relaying and RISs as two separate technologies, few works have demonstrated the benefits of integrating RISs in active relaying networks. In particular, the works in [9]–[13] have shown that RISs can considerably improve the effective rates of conventional relay-based networks. However, in all of these works the authors considered a conventional relay network with a single relay node aided by an RIS, and no SR or IRI was considered in any of these works. In contrast, in this work we investigate the performance of SR networks with the help of two RISs, where we jointly design the passive beamforming weights for the two RISs to provide a spatial (on the air) suppression of the IRI while maximizing the desired signals gains. Our contributions can be summarized as follows:

- We propose a new successive decode-and-forward (DF) relaying network with two RISs, and investigate its effective rate performance. The corresponding max-min optimization problem is formulated and solved via a semidefinite programming (SDP) approach.
- In addition, as SDP schemes are known to suffer from a high computational complexity, we propose an efficient evolutionary scheme based on particle swarm optimization (PSO) [14] to tackle the joint phase-shift design for both RISs. Furthermore, modifications of the PSO are proposed exploiting the structure of the problem to guarantee stability and control the speed and accuracy of convergence.
- Our results demonstrate that RISs can suppress IRI arising from the SR, and a large gain in achievable rates is obtained compared to the cases where only relays or RISs are utilized. Moreover, the proposed PSO scheme is shown to be highly efficient and can achieve a near-optimal performance when compared to the SDP solution.

It is worth highlighting that our proposed PSO scheme is novel in the sense that it was designed specifically to tackle the RIS passive beamforming with guaranteed stability and controlled convergence behavior.

The rest of this paper is organized as follows: The adopted

system model is introduced in Section II. Section III deals with the SDP-based beamforming design, while the PSO-based scheme is introduced and explained in detail in Section IV. Numerical results are presented and discussed in Section V. Finally, conclusions are drawn in Section VI.

Notations: Matrices and vectors are denoted by uppercase and lowercase boldface letters, respectively. $(\cdot)^*$, $(\cdot)^T$, and $(\cdot)^H$ denote the conjugate, transpose, and Hermitian transpose operators, respectively. In addition, \mathbf{a}_i , $[\mathbf{A}]_{:,j}$, and $[\mathbf{A}]_{i,j}$ are the i th row, j th column, and i th element of the j th column of \mathbf{A} , respectively, while $[\mathbf{x}]_i$ and x_i both represent the i th element of \mathbf{x} and used interchangeably as appropriate. $\mathbf{0}_{N \times M}$ and \mathbf{I}_N are the $N \times M$ all-zero and $N \times N$ identity matrices, respectively. Furthermore, $\text{diag}\{\mathbf{a}\}$ is a diagonal matrix whose diagonal is the elements of \mathbf{a} , while $\text{diag}\{\mathbf{A}\}$ is a vector whose elements are the diagonal elements of \mathbf{A} . The trace of \mathbf{A} is denoted by $\text{tr}(\mathbf{A})$, while $\mathbf{A} \succeq 0$ indicates that \mathbf{A} is a positive semidefinite matrix. Finally, $|\cdot|$ and $\mathbb{E}\{\cdot\}$ denote the absolute and expectation operators, respectively.

II. SYSTEM MODEL

We consider a time-division duplex scenario where a source node (S) transmits data to a destination node (D). Two HD-DF relays R_1 and R_2 , located between S and D , assist the communication by adopting SR to exploit the full bandwidth. Furthermore, two RISs denoted by I_1 and I_2 , located near R_1 and R_2 , respectively, are utilized to enhance the communication quality and suppress the IRI arising from the SR operation. We assume that each of S , D , R_1 and R_2 are equipped with a single omni-directional antenna, while I_1 and I_2 each has M reflective elements.

At any given transmission-time slot, one of the two relays operates as a receiver (Rx) to receive the new block of data from S , while the other relay operates as a transmitter (Tx) to forward the decoded message received from S in the previous time instant to D ; see Fig. 1.¹ Focusing on the case where R_1 operates as an Rx, and assuming that signals reflected from each RIS more than once have very low powers and thus can be neglected, we can write the received signal at R_1 as:

$$y_{r_1} = \sqrt{p_s} \left(h_{sr_1} + \mathbf{h}_{i_1 r_1}^T \Theta_1 \mathbf{h}_{s i_1} + \mathbf{h}_{i_2 r_1}^T \Theta_2 \mathbf{h}_{s i_2} \right) x + \sqrt{p_{r_2}} \left(h_{r_2 r_1} + \mathbf{h}_{i_1 r_1}^T \Theta_1 \mathbf{h}_{r_2 i_1} + \mathbf{h}_{i_2 r_1}^T \Theta_2 \mathbf{h}_{r_2 i_2} \right) \tilde{x} + w_{r_1}, \quad (1)$$

where p_s and p_{r_2} are the transmit powers of S and R_2 , respectively, $\Theta_1 \in \mathbb{C}^{M \times M}$ and $\Theta_2 \in \mathbb{C}^{M \times M}$ are the diagonal reflection matrices of I_1 and I_2 , respectively, while $h_{sr_1} \in \mathbb{C}$, $h_{r_2 r_1} \in \mathbb{C}$, $\mathbf{h}_{i_1 r_1} \in \mathbb{C}^{M \times 1}$, $\mathbf{h}_{s i_1} \in \mathbb{C}^{M \times 1}$, $\mathbf{h}_{i_2 r_1} \in \mathbb{C}^{M \times 1}$, $\mathbf{h}_{s i_2} \in \mathbb{C}^{M \times 1}$, $\mathbf{h}_{r_2 i_1} \in \mathbb{C}^{M \times 1}$, and $\mathbf{h}_{r_2 i_2} \in \mathbb{C}^{M \times 1}$ denote the channels between $S \rightarrow R_1$, $R_2 \rightarrow R_1$, $I_1 \rightarrow R_1$, $S \rightarrow I_1$, $I_2 \rightarrow R_1$, $S \rightarrow I_2$, $R_2 \rightarrow I_1$, and $R_2 \rightarrow I_2$, respectively.² Moreover, x and \tilde{x} are the information symbols transmitted

¹Note that during the first and last transmission time slots, only a single relay will be active and no IRI will be present. However, in this work we focus on the case where both relays are active.

²The different narrowband fading channels adopted in this work will be explained in detail in Section V.

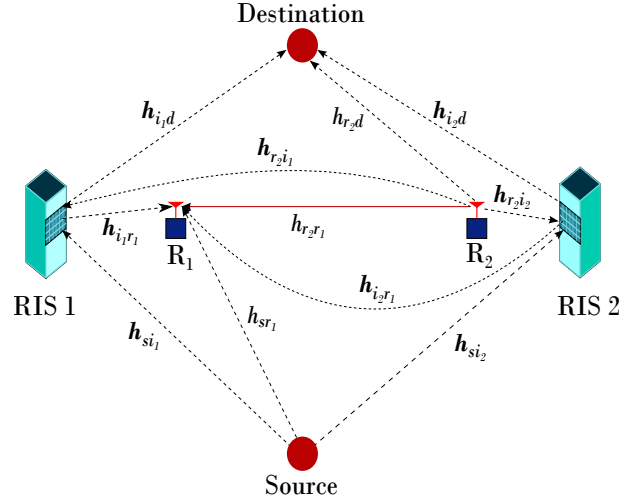


Fig. 1. The proposed RIS-enhanced SR scheme when R_1 operates as an Rx while R_2 operates as a Tx.

from S and R_2 , respectively, with $\mathbb{E}\{|x|^2\} = \mathbb{E}\{|\tilde{x}|^2\} = 1$, and $w_{r_1} \sim \mathcal{CN}(0, \sigma^2)$ is the additive white Gaussian noise (AWGN) at R_1 .³

For more convenience, we express the effective channels between each node (S , R_1 , and R_2) and the two RISs in a single vector. Specifically, we define $\mathbf{h}_{si} = \begin{bmatrix} h_{si1} \\ h_{si2} \end{bmatrix} \in \mathbb{C}^{2M \times 1}$, $\mathbf{h}_{ir1} = \begin{bmatrix} h_{i1r1} \\ h_{i2r1} \end{bmatrix} \in \mathbb{C}^{2M \times 1}$, $\mathbf{h}_{r2i} = \begin{bmatrix} h_{r2i1} \\ h_{r2i2} \end{bmatrix} \in \mathbb{C}^{2M \times 1}$, $\boldsymbol{\theta} = \begin{bmatrix} \boldsymbol{\theta}_1 \\ \boldsymbol{\theta}_2 \end{bmatrix} \in \mathbb{C}^{2M \times 1}$, where $\boldsymbol{\theta}_j = \text{diag}\{\Theta_j\}$ ($j \in \{1, 2\}$). Hence, the signal-to-interference plus noise ratio (SINR) at R_1 can be expressed as follows:

$$\gamma_{r_1} = \frac{p_s |h_{sr_1} + \mathbf{h}_{ir_1}^T \boldsymbol{\theta} \mathbf{h}_{si}|^2}{p_{r_2} |h_{r_2 r_1} + \mathbf{h}_{ir_1}^T \boldsymbol{\theta} \mathbf{h}_{r_2 i}|^2 + \sigma^2}, \quad (2)$$

where $\boldsymbol{\theta} = \text{diag}\{\boldsymbol{\theta}\} \in \mathbb{C}^{2M \times 2M}$. On the other hand, we can write the received signal at D (assuming no direct link between S and D exists except through the RISs) as follows:

$$y_d = \sqrt{p_{r_2}} \left(h_{r_2 d} + \mathbf{h}_{id}^T \boldsymbol{\theta} \mathbf{h}_{r_2 i} \right) \tilde{x} + \sqrt{p_s} \left(\mathbf{h}_{id}^T \boldsymbol{\theta} \mathbf{h}_{s i} \right) x + w_d, \quad (3)$$

where $\mathbf{h}_{id} = \begin{bmatrix} h_{i_1 d} \\ h_{i_2 d} \end{bmatrix} \in \mathbb{C}^{2M \times 1}$ is a vector containing the channel coefficients between D and both RISs, $h_{r_2 d}$ is the channel coefficient between R_2 and D , and $w_d \sim \mathcal{CN}(0, \sigma^2)$ is the AWGN at D . Noting that x represents interference to the destination in this case, we can write the SINR at D as:

$$\gamma_d = \frac{p_{r_2} |h_{r_2 d} + \mathbf{h}_{id}^T \boldsymbol{\theta} \mathbf{h}_{r_2 i}|^2}{p_s |\mathbf{h}_{id}^T \boldsymbol{\theta} \mathbf{h}_{s i}|^2 + \sigma^2}. \quad (4)$$

In the subsequent time-instant, S will transmit a new block of data to R_2 which will operate as an Rx, whereas R_1 will forward its received signal from S in the current time-slot,

³Throughout this work, we assume perfect channel state information (CSI) is available similar to [15] and [16]. Moreover, we assume a centralized processing such that all channels are known to either S or D in order to perform the joint phase-shift design.

assuming successful decoding, to D . Note that if the distances between $\{S, D\}$ and $\{R_i, I_i\}$ were the same for both $i \in \{1, 2\}$, then the system is symmetric, and thus it is sufficient to consider only a single phase to evaluate the achievable rate (in this case R_1 is the Rx while R_2 is the Tx). Therefore, as we adopt a symmetric system model in this work [17], we can write the effective rate at D , in bits/s/Hz, as follows:

$$\mathcal{R} = \min \{\log_2(1 + \gamma_{r_1}), \log_2(1 + \gamma_d)\}. \quad (5)$$

It is clear from (2) and (4) that the achievable rate depends on the reflection matrix Θ . In the next section, we formulate and solve the joint passive beamforming design problem by utilizing an SDP approach.

III. PASSIVE BEAMFORMING DESIGN VIA SEMIDEFINITE PROGRAMMING

In this section, we aim to maximize the achievable rate in (5) via an SDP approach. We start by formulating the corresponding optimization problem as follows:

$$\underset{\Theta}{\text{maximize}} \quad \min \{\log_2(1 + \gamma_{r_1}), \log_2(1 + \gamma_d)\} \quad (6)$$

subject to

$$|[\Theta]_{m,m}| = 1, \quad \forall m \in \mathcal{M}, \quad (6a)$$

where $\mathcal{M} = \{1, 2, \dots, 2M\}$. Due to the interference terms in (2) and (4), and the unit-modulus constraint on Θ in (6a), problem (6) is non-convex and cannot be solved in its current form in polynomial time. Therefore, in the following we adopt change of variables and introduce exponential slack variables to overcome the non-convexity of (6).

Let $\mathbf{q}_{sr_1} = \begin{bmatrix} \text{diag}\{\mathbf{h}_{ir_1}\}\mathbf{h}_{si} \\ h_{sr_1} \end{bmatrix}$, $\mathbf{q}_{r_2r_1} = \begin{bmatrix} \text{diag}\{\mathbf{h}_{ir_1}\}\mathbf{h}_{r_2i} \\ h_{r_2r_1} \end{bmatrix}$, $\mathbf{q}_{r_2d} = \begin{bmatrix} \text{diag}\{\mathbf{h}_{id}\}\mathbf{h}_{r_2i} \\ h_{r_2d} \end{bmatrix}$, $\mathbf{q}_{sd} = \begin{bmatrix} \text{diag}\{\mathbf{h}_{id}\}\mathbf{h}_{si} \\ 0 \end{bmatrix}$, and $\mathbf{v} = \begin{bmatrix} \theta \\ 1 \end{bmatrix}$. Moreover, by defining $\mathbf{Q}_{sr_1} = \mathbf{q}_{sr_1}\mathbf{q}_{sr_1}^H$, $\mathbf{Q}_{r_2r_1} = \mathbf{q}_{r_2r_1}\mathbf{q}_{r_2r_1}^H$, $\mathbf{Q}_{r_2d} = \mathbf{q}_{r_2d}\mathbf{q}_{r_2d}^H$, $\mathbf{Q}_{sd} = \mathbf{q}_{sd}\mathbf{q}_{sd}^H$, and $\mathbf{V} = \mathbf{v}\mathbf{v}^T$, we can now equivalently represent γ_{r_1} and γ_d as follows:

$$\gamma_{r_1} = \frac{p_s \text{tr}(\mathbf{V}\mathbf{Q}_{sr_1})}{p_{r_2} \text{tr}(\mathbf{V}\mathbf{Q}_{r_2r_1}) + \sigma^2}, \quad (7a)$$

$$\gamma_d = \frac{p_{r_2} \text{tr}(\mathbf{V}\mathbf{Q}_{r_2d})}{p_s \text{tr}(\mathbf{V}\mathbf{Q}_{sd}) + \sigma^2}. \quad (7b)$$

However, even with relaxing the rank-one constraint on \mathbf{V} , formulating the max-min optimization problem with the current formulations of γ_{r_1} and γ_d would still result in a non-convex objective function. Nonetheless, this can now be dealt with by introducing additional slack variables [18]. In particular, let $\mathbf{s} = [s_1 \ s_2]^T$ and $\mathbf{u} = [u_1 \ u_2]^T$ be exponential slack variables such that

$$p_s \text{tr}(\mathbf{V}\mathbf{Q}_{sr_1}) + p_{r_2} \text{tr}(\mathbf{V}\mathbf{Q}_{r_2r_1}) + \sigma^2 = e^{s_1}, \quad (8a)$$

$$p_{r_2} \text{tr}(\mathbf{V}\mathbf{Q}_{r_2r_1}) + \sigma^2 = e^{u_1}, \quad (8b)$$

$$p_{r_2} \text{tr}(\mathbf{V}\mathbf{Q}_{r_2d}) + p_s \text{tr}(\mathbf{V}\mathbf{Q}_{sd}) + \sigma^2 = e^{s_2}, \quad (8c)$$

$$p_s \text{tr}(\mathbf{V}\mathbf{Q}_{sd}) + \sigma^2 = e^{u_2}. \quad (8d)$$

Subsequently, and after dropping the rank-one constraint on \mathbf{V} via semidefinite relaxation [19], we can introduce the following optimization problem⁴

$$\underset{s_1, s_2, u_1, u_2, \mathbf{V}}{\text{maximize}} \quad \min_{i \in \{1, 2\}} \{s_i - u_i\} \quad (9)$$

subject to

$$p_s \text{tr}(\mathbf{V}\mathbf{Q}_{sr_1}) + p_{r_2} \text{tr}(\mathbf{V}\mathbf{Q}_{r_2r_1}) + \sigma^2 \geq e^{s_1}, \quad (9a)$$

$$p_{r_2} \text{tr}(\mathbf{V}\mathbf{Q}_{r_2r_1}) + \sigma^2 \leq e^{u_1}, \quad (9b)$$

$$p_{r_2} \text{tr}(\mathbf{V}\mathbf{Q}_{r_2d}) + p_s \text{tr}(\mathbf{V}\mathbf{Q}_{sd}) + \sigma^2 \geq e^{s_2}, \quad (9c)$$

$$p_s \text{tr}(\mathbf{V}\mathbf{Q}_{sd}) + \sigma^2 \leq e^{u_2}, \quad (9d)$$

$$[\mathbf{V}]_{m,m} = 1, \quad m \in \{1, 2, \dots, 2M + 1\}, \quad (9e)$$

$$\mathbf{V} \succeq 0. \quad (9f)$$

The only non-convex constraints at this stage are (9b) and (9d). To overcome this drawback, a first-order Taylor approximation is applied to convert these constraints into convex ones. In particular, we define $\bar{\mathbf{u}} = [\bar{u}_1 \ \bar{u}_2]^T$, where \bar{u}_1 and \bar{u}_2 are the points around which the linearization is made such that $e^{u_i} \approx e^{\bar{u}_i}(u_i - \bar{u}_i + 1)$. Hence, we can recast problem (9) as

$$\underset{s_1, s_2, u_1, u_2, \mathbf{V}}{\text{maximize}} \quad \min_{i \in \{1, 2\}} \{s_i - u_i\} \quad (10)$$

subject to

$$p_{r_2} \text{tr}(\mathbf{V}\mathbf{Q}_{r_2r_1}) + \sigma^2 \leq e^{\bar{u}_1}(u_1 - \bar{u}_1 + 1), \quad (10a)$$

$$p_s \text{tr}(\mathbf{V}\mathbf{Q}_{sd}) + \sigma^2 \leq e^{\bar{u}_2}(u_2 - \bar{u}_2 + 1), \quad (10b)$$

$$\text{and constraints (9a), (9c), (9e), and (9f)}. \quad (10c)$$

It follows that all constraints and objective function at this stage are convex, and problem (10) can be solved iteratively using software tools such as CVX. However, we firstly initialize \bar{u}_1 and \bar{u}_2 as follows

$$\bar{u}_1^{(0)} = \ln(p_{r_2} \text{tr}(\tilde{\mathbf{V}}\mathbf{Q}_{r_2r_1}) + \sigma^2), \quad (11a)$$

$$\bar{u}_2^{(0)} = \ln(p_s \text{tr}(\tilde{\mathbf{V}}\mathbf{Q}_{sd}) + \sigma^2), \quad (11b)$$

where $\tilde{\mathbf{V}}$ is any feasible (i.e. random) solution. Once the algorithm has converged, there is no guarantee that the rank of \mathbf{V}^* is equal to 1. In such case, the value of the objective function corresponding to \mathbf{V}^* represents an upper-bound. Nonetheless, one can apply eigenvalue decomposition (EVD) with Gaussian randomization to approximate a rank-1 near optimal solution [20]. The details are omitted here for brevity, however, it is worth pointing out that such approximation guarantees a minimum accuracy of $\pi/4$ of the optimal objective value [21]. The steps of the proposed scheme are given in Algorithm 1.

IV. PARTICLE SWARM OPTIMIZATION-BASED BEAMFORMING DESIGN

The main drawback for the SDP approach is that it suffers from a complexity order of $\mathcal{O}((2M + 1)^{3.5})$ [22], and hence, it becomes unsuitable when dealing with large optimization problems. Therefore, in this section we propose a lower-complexity evolutionary method to tackle the phase-shift design, which is based on PSO [14].

⁴It is worth highlighting that $\frac{1}{\ln(2)}$ is omitted from the objective function without any loss of optimality.

Algorithm 1 Proposed SDP algorithm for phase-shifts design

- 1: **input** $\mathbf{Q}_{sr_1}, \mathbf{Q}_{r_2r_1}, \mathbf{Q}_{r_2d}, \mathbf{Q}_{sd}, p_s, p_{r_2}, \sigma^2, \bar{u}_1^{(0)}, \bar{u}_2^{(0)}, \epsilon = 10^{-3}$ (accuracy), $k = 1$ (iteration index),
 - 2: **define** $\text{err}^{(k)} \triangleq \sum_{i=1}^2 |u_i^{(k)} - \bar{u}_i^{(k-1)}|$
 - 3: **repeat**
 - 4: **solve** (10) and then **evaluate** $\text{err}^{(k)}$,
 - 5: **if** $\text{err}^{(k)} < \epsilon$
 - 6: **break**;
 - 7: **else update** $\bar{u}^{(k)} := u^{(k)}$, and then **increment** $k := k+1$,

 - 8: **until** convergence
-

We start by generating an initial population of N particles $\mathbf{F} = [\mathbf{f}_1, \mathbf{f}_2, \dots, \mathbf{f}_N]^T \in \mathbb{R}^{N \times 2M}$ with entries (or phase-shifts) drawn randomly in the interval $[-\pi, \pi]$. We evaluate the fitness of the n th particle (λ_n) as follows:

$$\lambda_n = \min \left\{ \gamma_{r_1}(\mathbf{f}_n), \gamma_d(\mathbf{f}_n) \right\}, \quad \forall n \in \{1, \dots, N\}, \quad (12)$$

where $\gamma_{r_1}(\mathbf{f}_n)$ and $\gamma_d(\mathbf{f}_n)$ are the SINR values at R_1 and D given in (2) and (4), respectively, such that

$$\gamma_i(\mathbf{f}_n) = \left\{ \gamma_i \mid \Theta = \text{diag}\{e^{j\mathbf{f}_n}\} \right\}, i \in \{r_1, d\}. \quad (13)$$

Then, we find the *local best* and *global best* solutions. Specifically, the *global best* solution for the m th element of each particle is the m th entry of the particle that has the highest fitness value in the population. Thus, the vector of global best solutions is in fact the particle that has the highest fitness in the population, which we denote as \mathbf{f}_{\max} .

In contrast, the *local best* solution for the m th element of \mathbf{f}_n , denoted by $[\mathbf{L}]_{n,m}$ ($\mathbf{L} \in \mathbb{R}^{N \times 2M}$), is the m th entry of the particle with the highest fitness value among only the neighbouring particles of \mathbf{f}_n , which are \mathbf{f}_{n+1} and \mathbf{f}_{n-1} .⁵

Furthermore, the velocities that control the direction of each particle, which we initialize as $\mathbf{X} = \mathbf{0}_{N \times 2M}$, are updated at each iteration as follows [14]

$$\begin{aligned} [\mathbf{X}^{(t+1)}]_{n,m} &= [\mathbf{X}^{(t)}]_{n,m} + w_1 r_1 \left([\mathbf{L}]_{n,m} - [\mathbf{F}^{(t)}]_{n,m} \right) \\ &+ w_2 r_2 \left([\mathbf{f}_{\max}]_m - [\mathbf{F}^{(t)}]_{n,m} \right), n \in \mathcal{N}, m \in \mathcal{M}. \end{aligned} \quad (14)$$

where w_1 and w_2 are learning factors, r_1 and r_2 are random numbers drawn from a uniform distribution with values between 0 and 1, and $\mathcal{N} = \{1, \dots, N\}$. To ensure a stable convergence,⁶ we normalize each column of $\mathbf{X}^{(t+1)}$ as

$$[\mathbf{X}^{(t+1)}]_{:,m} := \mu \times \frac{[\mathbf{X}^{(t+1)}]_{:,m}}{\max \left\{ \left| [\mathbf{X}^{(t+1)}]_{:,m} \right| \right\}}, \quad (15)$$

where $\mu \in (0, \pi]$ is an introduced (auxiliary) parameter. Then, the phase-shifts are updated as

$$\mathbf{F}^{(t+1)} = \mathbf{F}^{(t)} + \mathbf{X}^{(t+1)}. \quad (16)$$

⁵We adopt a ring topology, thus, the neighbouring particles for \mathbf{f}_1 are \mathbf{f}_2 and \mathbf{f}_N , while the neighbours of \mathbf{f}_N are \mathbf{f}_1 and \mathbf{f}_{N-1} .

⁶Note that performing the normalization in (15) is crucial, and without it the values of \mathbf{X} can become extremely large (or small) after many iterations, preventing the algorithm from finding any good solution.

Algorithm 2 Proposed PSO algorithm for phase-shifts design

- 1: **input** \mathbf{F} (initial population), \mathbf{X} (initial velocities), $t = 0$, T (maximum number of iterations), and μ ,
 - 2: **while** $t \leq T$
 - 3: **evaluate** the fitness of each particle in \mathbf{F} ,
 - 4: **find** *global best* and *local best* solutions,
 - 5: **update** the velocities according to (14),
 - 6: **normalize** the new velocities according to (15),
 - 7: **update** the population according to (16),
 - 8: **adjust** the new population according to (17),
 - 9: **increment** $t := t + 1$,
 - 10: **end while**
 - 11: **output**: particle with highest fitness value.
-

It is worth to highlight that the value of μ in (15) controls the speed and accuracy of convergence, and it represents the highest possible phase-shift difference per reflecting element between any two successive iterations. Finally, we re-adjust the entries of $\mathbf{F}^{(t+1)}$ that are either greater than π or less than $-\pi$. Due to the circular symmetry of phase-shifts, the re-adjustment can be carried out as follows

$$[\mathbf{F}^{(t+1)}]_{n,m} := \begin{cases} [\mathbf{F}^{(t+1)}]_{n,m} + 2\pi, & \text{if } [\mathbf{F}^{(t+1)}]_{n,m} < -\pi \\ [\mathbf{F}^{(t+1)}]_{n,m} - 2\pi, & \text{if } [\mathbf{F}^{(t+1)}]_{n,m} > \pi. \end{cases} \quad (17)$$

As shown in Algorithm 2, the same procedure (i.e. fitness evaluation, obtaining *local best* and *global best* solutions, update of velocities followed by normalization, update of phase-shifts of the population, and re-adjustment) will be repeated in subsequent iterations until a maximum number of iterations is reached, and the particle that achieves the highest fitness value in all $t \in \{0, 1, \dots, T-1\}$ iterations will be selected as the final solution.

When it comes to the per-iteration complexity of the proposed PSO scheme, we can observe that the (fitness evaluation, update of velocity, normalization, update of population, and adjustment), each has a complexity order of $\mathcal{O}(2MN)$. Thus, and compared to the SDP approach, the PSO becomes particularly attractive when dealing with a large number of reflecting elements, as its complexity scales only linearly with the size of optimization problem.

V. RESULTS AND DISCUSSION

We start by introducing the different narrowband channels and parameters involved in this paper. All channels from and to each RIS are assumed to follow Rician distribution with both line-of-sight (LoS) and non-LoS (NLoS) links, such that $\mathbf{h}_j = \sqrt{\frac{k_r}{k_r+1}} \mathbf{h}_j^{\text{los}} + \sqrt{\frac{1}{1+k_r}} \mathbf{h}_j^{\text{nlos}}$, where k_r is the Rician K factor, $\mathbf{h}_j^{\text{los}} \in \mathbb{C}^{M \times 1}$ is the deterministic LoS channel vector for the j th link, with each element having an absolute value of $1/d_j^{\alpha_{\text{los}}/2}$ and a random phase between 0 and 2π , $\mathbf{h}_j^{\text{nlos}} \sim \mathcal{CN}(\mathbf{0}_{M \times 1}, \mathbf{I}_M d_j^{-\alpha_{\text{nlos}}})$ is the Rayleigh distributed NLoS channel vector, where d_j is the distance between the nodes associated with the j th link, $j \in$

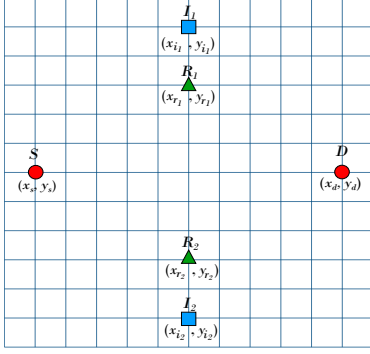


Fig. 2. A top-view of the adopted simulation setup.

$\{s i_1, i_1 r_1, r_2 i_1, i_1 d, s i_2, i_2 r_1, r_2 i_2, i_2 d\}$, while α_{los} and α_{nlos} represent the path-loss exponents for LoS and NLoS links, respectively. In contrast, $h_i \sim \mathcal{CN}(0, d_i^{-\alpha_{\text{nlos}}})$ represents the channel coefficient with Rayleigh distribution for links that do not involve any of the RISs, i.e. $i \in \{s r_1, r_2 d\}$. However, for the IRI link, $h_{r_2 r_1}$, we consider Rician channel to demonstrate the efficiency of RISs in suppressing the interference even when a strong LoS channel exists.

The locations of different nodes are set as: $(x_s, y_s) = (0, 0)$, $(x_d, y_d) = (100, 0)$, $(x_{r_1}, y_{r_1}) = (50, 25)$, $(x_{r_2}, y_{r_2}) = (50, -25)$, $(x_{i_1}, y_{i_1}) = (50, 30)$, and $(x_{i_2}, y_{i_2}) = (50, -30)$, all in meter units, see Fig. 2. In addition, we set $w_1 = w_2 = 2$, $\sigma^2 = 1$, $k_r = 5$ dB, $\alpha_{\text{los}} = 2.3$, and $\alpha_{\text{nlos}} = 3.5$. Equal power allocation was utilized and thus $p_s = p_{r_2} = \frac{1}{2}p$, and we define the transmit signal-to-noise ratio (SNR) as p/σ^2 .

Our simulations compare between the following schemes:

- **RISs-assisted SR (upper-bound):** This refers to the results obtained by SDP without performing EVD with Gaussian randomization, hence, the term upper-bound. Rician fading is assumed for the IRI channel (i.e. $h_{r_2 r_1}$).
- **SR without RISs:** This case demonstrates the results for SR utilizing only the two relays without the RISs. Rayleigh fading is adopted for all different channels including the IRI link.
- **RISs only:** In this case, we only have two RISs (therefore no SR) and we optimize their phase-shifts to reflect the signal from S toward D , where the former transmits with a power budget of p Watts.
- **RISs-assisted SR (PSO):** This case shows the performance of our proposed PSO scheme, assuming Rician-fading for the IRI link.

In Fig. 3, we depict the achievable rate vs. SNR curves. The RISs-assisted SR notably outperforms both cases of RISs-only scheme and the SR case without RISs. In particular, to achieve an effective rate of 4 bits/s/Hz, a gain of 15 dB in transmit SNR can be obtained for the proposed RISs-assisted SR over the RISs-only approach, given that the number of reflecting elements per RIS is 32. In contrast, the SR case without RISs shows a very poor performance, which highlights the severe

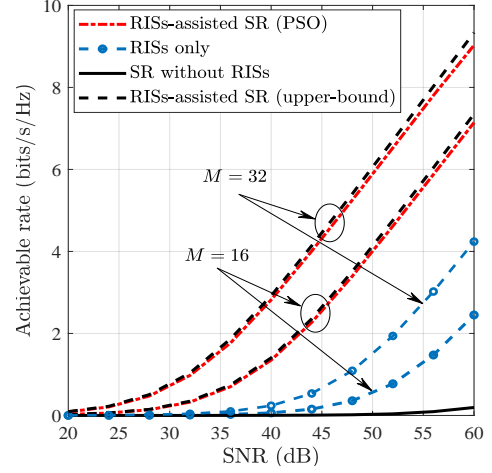


Fig. 3. Achievable rate vs transmit SNR for different schemes when $N = 100$, $T = 200$, and $\mu = \pi/8$.

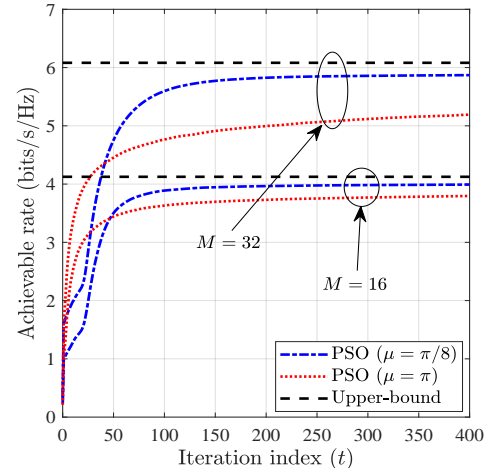


Fig. 4. Convergence behavior of the proposed PSO when $N = 50$, and transmit SNR = 50 dB.

impact of the IRI. Moreover, one can also observe from Fig. 3 that there is only a negligible performance gap between the low-complexity PSO scheme and the more complex SDP approach.

In Fig. 4, we show the convergence behavior of the proposed PSO scheme for different number of reflecting elements and different values of the auxiliary parameter μ . Regardless of the number of reflecting elements, setting μ to a small value (in this case $\pi/8$) is preferable as it allows the proposed algorithm to converge toward better solutions that are close to the optimal points. In contrast, larger values of μ enable faster exploration of new and more diverse populations, and thus they are preferable when the number of optimization iterations is small. However, they are more likely to fail in finding near optimal solutions due to the rapid velocity changes of candidate particles, especially when the number of reflecting elements is relatively large.

VI. CONCLUSION

In this work, a new RIS-aided relay network architecture was proposed with SR, where two RISs were deployed near the two HD-DF relays to provide a spatial suppression of IRI while maximizing the gain of desired signals. An upper bound solution for the achievable rate was obtained via the SDP technique without performing Gaussian randomization and EVD. Subsequently, a lower-complexity beamforming design based on PSO with controlled convergence speed was proposed, and a new normalization step was introduced which guaranteed the stability of the designed scheme. Numerical results demonstrated that RISs can provide large improvements on the rate performance of SR networks, even when a strong line-of-sight link for the IRI existed. Finally, the proposed PSO scheme showed its capability in obtaining near optimal solutions.

ACKNOWLEDGMENT

This work was supported by the Luxembourg National Research Fund (FNR) under the CORE project RISOTTI.

REFERENCES

- [1] Y. Fan, C. Wang, J. Thompson, and H. V. Poor, "Recovering multiplexing loss through successive relaying using repetition coding," *IEEE Trans. Wireless Commun.*, vol. 6, no. 12, pp. 4484–4493, Dec. 2007.
- [2] W. Chen, "CAO-SIR: Channel aware ordered successive relaying," *IEEE Trans. Wireless Commun.*, vol. 13, no. 12, pp. 6513–6527, Dec. 2014.
- [3] H. Wicaksana, S. H. Ting, C. K. Ho, W. H. Chin, and Y. L. Guan, "AF two-path half duplex relaying with inter-relay self interference cancellation: Diversity analysis and its improvement," *IEEE Trans. Wireless Commun.*, vol. 8, no. 9, pp. 4720–4729, Sep. 2009.
- [4] A. Ikhlef, J. Kim, and R. Schober, "Mimicking full-duplex relaying using half-duplex relays with buffers," *IEEE Trans. Veh. Technol.*, vol. 61, no. 7, pp. 3025–3037, Sep. 2012.
- [5] X. Tan, Z. Sun, J. M. Jornet, and D. Pados, "Increasing indoor spectrum sharing capacity using smart reflect-array," in *IEEE Inter. Conf. Commun. (ICC)*, Kuala Lumpur, Malaysia, May 2016, pp. 1–6.
- [6] N. Rajatheva, I. Atzeni, E. Bjornson, A. Bourdoux *et al.*, "White paper on broadband connectivity in 6G," [Online]. Available: <https://arxiv.org/abs/2004.14247>, 2020.
- [7] M. Z. Chowdhury, M. Shahjalal, S. Ahmed, and Y. M. Jang, "6G wireless communication systems: Applications, requirements, technologies, challenges, and research directions," *IEEE Open J. Commun. Soc.*, vol. 1, pp. 957–975, Aug. 2020.
- [8] S. Kisseleff, W. A. Martins, H. Al-Hraishawi, S. Chatzinotas, and B. Ottersten, "Reconfigurable intelligent surfaces for smart cities: Research challenges and opportunities," *IEEE Open J. Commun. Soc.*, vol. 1, pp. 1781–1797, Dec. 2020.
- [9] Z. Abdullah, G. Chen, S. Lambotharan, and J. A. Chambers, "A hybrid relay and intelligent reflecting surface network and its ergodic performance analysis," *IEEE Wireless Commun. Lett.*, vol. 9, no. 10, pp. 1653–1657, Oct. 2020.
- [10] —, "Optimization of intelligent reflecting surface assisted full-duplex relay networks," *IEEE Wireless Commun. Lett.*, vol. 10, no. 2, pp. 363–367, Feb. 2021.
- [11] J. Wang, Y.-C. Liang, J. Joung, X. Yuan, and X. Wang, "Joint beamforming and reconfigurable intelligent surface design for two-way relay networks," *IEEE Trans. Commun.*, To appear.
- [12] I. Yildirim, F. Kilinc, E. Basar, and G. C. Alexandropoulos, "Hybrid RIS-empowered reflection and decode-and-forward relaying for coverage extension," *IEEE Commun. Lett.*, vol. 25, no. 5, pp. 1692–1696, May 2021.
- [13] M. Obeed and A. Chaaban, "Joint beamforming design for multiuser MISO downlink aided by a reconfigurable intelligent surface and a relay," [Online]. Available: <https://arxiv.org/abs/2104.08417>, 2021.
- [14] J. Kennedy and R. Eberhart, "Particle swarm optimization," in *Proc. IEEE Int. Conf. Neural Networks*, Perth, Australia, Nov. 1995, pp. 1942–1948.
- [15] Q. Wu and R. Zhang, "Intelligent reflecting surface enhanced wireless network via joint active and passive beamforming," *IEEE Trans. Wireless Commun.*, vol. 18, no. 11, pp. 5394–5409, Nov. 2019.
- [16] C. Huang, A. Zappone, G. C. Alexandropoulos, M. Debbah, and C. Yuen, "Reconfigurable intelligent surfaces for energy efficiency in wireless communication," *IEEE Trans. Wireless Commun.*, vol. 18, no. 8, pp. 4157–4170, Aug. 2019.
- [17] R. Zhang, "On achievable rates of two-path successive relaying," *IEEE Trans. Commun.*, vol. 57, no. 10, pp. 2914–2917, Oct. 2009.
- [18] P. Zhao, M. Zhang, H. Yu, H. Luo, and W. Chen, "Robust beamforming design for sum secrecy rate optimization in MU-MISO networks," *IEEE Trans. Inf. Forensics Security*, vol. 10, no. 9, pp. 1812–1823, Sep. 2015.
- [19] Z.-Q. Luo, W.-K. Ma, A. M.-C. So, Y. Ye, and S. Zhang, "Semidefinite relaxation of quadratic optimization problems," *IEEE Sig. Process. Mag.*, vol. 27, no. 3, pp. 20–34, May 2010.
- [20] Q. Wu and R. Zhang, "Intelligent reflecting surface enhanced wireless network: Joint active and passive beamforming design," in *IEEE Global Commun. Conf. (GLOBECOM)*, Abu Dhabi, UAE, Dec. 2018, pp. 1–6.
- [21] S. Zhang and Y. Huang, "Complex quadratic optimization and semidefinite programming," *SIAM J. Optim.*, vol. 16, no. 3, pp. 871–890, 2006.
- [22] M. Cui, G. Zhang, and R. Zhang, "Secure wireless communication via intelligent reflecting surface," *IEEE Wireless Commun. Lett.*, vol. 8, no. 5, pp. 1410–1414, Oct. 2019.